Applied Energy 228 (2018) 1486–1498

Contents lists available at ScienceDirect

Applied Energy

journal homepage: www.elsevier.com/locate/apenergy

Feasibility study about using a stand-alone wind power driven heat pump for space heating

Hailong Li[a,b,c], Pietro Elia Campana[a,b,d,*], Yuting Tan[a,d], Jinyue Yan[b,d]

[a] Ningbo RX New Materials Tch. Co. Ltd., Ningbo 315200, China
[b] Future Energy, School of Business, Society and Engineering, Mälardalen University, 72123 Västerås, Sweden
[c] Tianjin Key Laboratory of Refrigeration Technology, Tianjin University of Commerce, Tianjin 300134, China
[d] Department of Chemical Engineering, KTH Royal Institute of Technology, 10044 Stockholm, Sweden

HIGHLIGHTS

- This study studies a heat pump system directly coupled with a wind turbine for a detached house.
- The intermittency of wind energy results in significant thermal discomfort.
- Increasing the capacity of wind turbines does not necessarily lead to an improved thermal comfort.
- The battery system can effectively lower the loss of load probability.
- The time interval used in the dynamic simulation has significant influence on the results.

ARTICLE INFO

Keywords:
Wind power
Heat pump
Dynamic performance
Space heating
Standalone system
Loss of load probability
Sweden

ABSTRACT

Reducing energy consumption and increasing the use of renewable energy in the building sector are crucial to the mitigation of climate change. Wind power driven heat pumps have been considered as a sustainable measure to supply heat to the detached houses, especially those that even do not have access to the electricity grid. This work is to investigate the dynamic performance of a heat pump system driven by wind turbine through dynamic simulations. In order to understand the influence on the thermal comfort, which is the primary purpose of space heating, the variation of indoor temperature has been simulated in details. Results show that the wind turbine is not able to provide the electricity required by the heat pump during the heating season due to the intermittent characteristic of wind power. To improve the system performance, the influences of the capacity of wind turbine, the size of battery and the setpoint of indoor temperature were assessed. It is found that increasing the capacity of wind turbines is not necessary to reduce the loss of load probability; while on the contrary, increasing the size of battery can always reduce the loss of load probability. The setpoint temperature clearly affects the loss of load probability. A higher setpoint temperature results in a higher loss of thermal comfort probability. In addition, it is also found that the time interval used in the dynamic simulation has significant influence on the result. In order to have more accurate results, it is of great importance to choose a high resolution time step to capture the dynamic behaviour of the heat supply and its effect on the indoor temperature.

1. Introduction

Currently, the building sector has consumed more energy than the industry sector, the transport sector, the agriculture and non-energy use sector, accounting for more than one third of the world's energy consumption [1]; and more than 50% is used for space heating and cooling [2]. In Sweden, the energy consumption for space heating and domestic hot water (DHW) production reached 100 TWh in 2014 [3]. Sweden has already set a target to reduce it by 20% by 2020 and 50% by 2050 comparing to the level in 1995 [4]. To achieve a sustainable development, reducing energy consumption in the building sector is playing an important role.

In Sweden, there are different ways to supply heat, such as district heating (DH), heat pumps (HPs), electrical radiator, and biomass/oil/gas boilers. Even though, DH is the most common way to supply heat, accounting for more than 50% of the total heat demand, there are still

* Corresponding author at: Ningbo RX New Materials Tch. Co. Ltd., Ningbo 315200, China; Future Energy, School of Business, Society and Engineering, Mälardalen University, 72123 Västerås, Sweden; Department of Chemical Engineering, KTH Royal Institute of Technology, 10044 Stockholm, Sweden.
E-mail address: pietro.campana@mdh.se (P.E. Campana).

https://doi.org/10.1016/j.apenergy.2018.06.146
Received 8 January 2018; Received in revised form 23 June 2018; Accepted 30 June 2018
Available online 18 July 2018
0306-2619/

many single family houses that are not connected the DH network. HPs represent an energy efficiency technology for heat production; however, the share of HPs in the Swedish heat market is not very high, only covering a little more than 20% of the heat demand. Meanwhile, although there is a tiny share of power from fossil fuel in Sweden, nuclear power accounts for a big proportion, more than 40% [5]. Nevertheless, nuclear power is planned to be phased out in Sweden, therefore, more power should be explored from other renewable resources, such as wind power. Wind power has experienced a fast growth in the past 10 years. The installed capacity in 2016 was more than 10 times of that in 2004, reaching 6.5 GW and the produced power was 15.4 TWh [5]. Since wind potential is usually high during winter, in which the heat demand is high, using wind power to drive HPs is a proper technical solution and will be of significance to achieve the Swedish energy target in 2020 and 2050.

Some works have been done to evaluate the potential of using wind power to drive HPs. Waite and Modi evaluated the effects of coupling large-scale wind power installations in New York State with increased use of electric heat pumps to meet a portion of space heating and DHW demands in New York City [6]. Results showed significant increases in wind-generated electricity utilization with increased use of HPs, allowing for a higher installed capacity of wind power. Hedegaard et al. analyzed how the heat pumps can influence the integration of wind power by applying an energy system model that optimized both the investment and operation, and covered various heat storage options [7]. It was found that the HPs can contribute significantly to facilitating larger wind power investments in net zero energy settlements and reducing system costs, fuel consumption, and CO_2 emissions. Meibom et al. technologically and economically analyzed the integration of HPs with wind power [8], showing that the introduction of HPs was beneficial as the curtailment of wind power production was reduced, the price of regulating power was reduced and the hours with very low power prices were reduced. Warmer et al. investigated the performance of a heat pump integrated with wind power based on performed field test. Results showed that by making use of large buffering capacity in a number of installations large parts of the wind power fluctuations can be eliminated [9]. Fischer and Madani investigated HP systems in smart grid [10]. The results suggested that the integration of wind power on building level can be supported by HPs and the required electricity from the grid can be reduced by up to 95%. Poulet and Outbib concluded that heat pumps, operated in an optimal way, can be used to increase the absorption of wind power while at the same time reducing the need for peak capacity and thus costs [11].

Moreover, for detached houses that even do not have access to the electricity grid, HPs that are directly coupled with wind turbines (WT-HP) are more attractive [12]. There are some studies about developing WT-HPs. Jwo et al. have experimentally investigated the performance of a WT-HP system, proposing a method to improve the energy efficiency [13]. Other works [14–16] have also been conducted to investigate the dynamic performance of WT-HP, most of which focus on the system itself, such as the coefficient of performance (COP) and heat production, even though the detailed heat demand was not integrated. However, due to the intermittent characteristic of wind power, even though an energy storage is considered, there is no guarantee of a satisfying indoor thermal comfort when a standalone system is used. Therefore, to study the feasibility of WT-HP, it is essential to evaluate the system based on the real dynamic demand. Papaefthymiou et al. presented a methodology for the quantification of the flexibility offered by the thermal storage of building stock equipped with HPs, to power systems with significant penetration of wind power [12]. Li et al. proposed an hour-ahead heating strategy scheduling mode to accommodate curtailed wind power with a typical wind power output profile [17]. Østergaard analyzed and compared compression HPs and geothermal absorption HPs integrated with wind power in EnergyPLAN [18]. Many studies have been carried out regarding hybrid systems, which do not only consist of wind power. Poulet and Outbib studied energy conversion for dwellings by using hybrid systems based on HP variable input power [11]. Both wind power and PV were included. Sichilalu et al. studied a PV-wind-fuel cell-HP hybrid system that can produce both electricity and heat [19]. An optimal energy management strategy was proposed to minimize energy cost and maximize fuel cell output. The same authors also develops an optimal control model of a HP water heater (HPWH) supplied by a wind generator-photovoltaic-grid system [20]. Whereas, it was assumed that the demand can be fully satisfied by the hybrid system. Few studies have been done only for WT-HP. Chemekov and Kharchenko designed a WT-HP system to supply heat for an individual dwelling house with a total area of 295 m^2 situated in the city of Tuapse, Russia [21]. Both thermal energy storage and electricity storage were involved. Due to the fluctuation of wind power output, the mismatch between heat demand and heat supply was identified. Nevertheless, no results about indoor temperature were given.

Recent studies have focused the interest on the coupling of HPs and solar PV systems for space heating thanks to the drastic reduction of PV module prices [22,23]. Nevertheless, the major challenge for PV systems when used for space heating applications is the mismatch between heating load and PV production. In this perspective, despite the higher investment costs, small WTs can play an important role in space heating. This can be clearly understood when comparing the mutual relationships between ambient temperature vs global horizontal radiation and wind speed (at 10 m height), as shown in Fig. 1a and b. However, according to the literature review, there has been little information about the thermal comfort when a standalone WT-HP is used to supply heat to a detached house. Since the primary purpose of space heating is to provide a good thermal comfort, only assessing how much heat demand can be covered by a WT-HP is not sufficient to justify the feasibility. There is also a lack of knowledge about how to improve the thermal comfort when WT-HP is adopted. In addition, it is common to assume that the indoor temperature is constant when estimating the

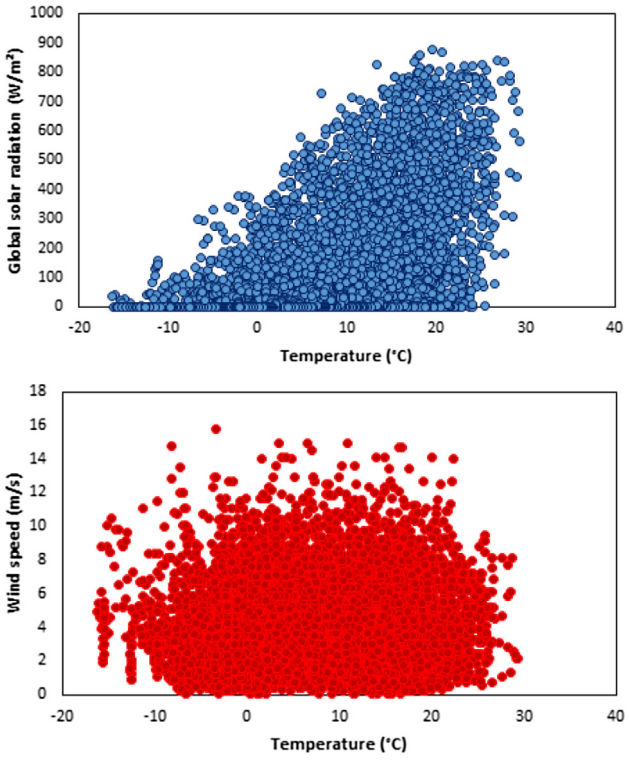

Fig. 1. (a) ambient temperature vs global solar radiation (up), and (b) ambient temperature vs wind speed (at 10 m height) (down) (the weather data refer to Stockholm (59.33 N, 18.06 E) and were retrieved from Meteonorm database [24]).

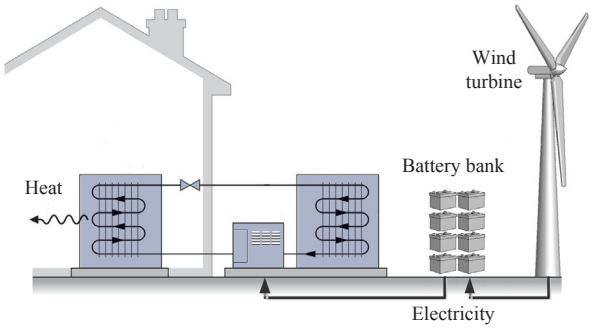

Fig. 2. Standalone wind power driven heat pump.

heat demand. However, for the detached houses equipped with a standalone WT-HP, the indoor temperature can fluctuate obviously, which can reversely affect the heat demand. Whereas, this has not been well considered in previous modelling and simulations.

In order to bridge the identified knowledge gaps, the dynamic heat supply and heat demand were modelled in details in this study. The fluctuation of indoor temperature was carefully calculated. In order to assess the thermal comfort, two key performance indicators have been proposed: the loss of load probability (LOLP) and the loss of thermal comfort probability (LOTCP). The results will provide insights and guidelines concerning the development of the standalone WT-HP and synergies between heating and electricity networks for space heating in detached houses.

2. Methodology

2.1. System description

As shown in Fig. 2, a HP system coupled with a standalone WT is used to supply heat to a detached house. To handle the intermittent characteristic of wind power, an electric energy storage system was included. In this work, it was assumed that heat is only supplied from October to March.

2.2. House model

A typical Swedish detached house model is built in TRNSYS® [25], a software for simulating the behaviour of transient systems, to define the dynamic heat demand. The main components for simulating the building heating load are: the weather data input block (Type 15 of the TRNSYS® library), the building model (Type 12), four window models (Type 35a) for the solar heat gains from the four building surfaces, a data reader block (Type 9) for the computed internal gains from lights, appliances and occupants, and an on/off differential controller (Type 2). The house is assumed to be located in Stockholm (59.33 N, 18.06 E) and south facing. It composes of two floors, including one living room, one kitchen, one laundry, two bathrooms, one office, two single rooms, one double bedroom, one hall way and one relax room, and has a total area of 153 m^2. Some general information about the house is listed in Table 1. The sizes of the front and back doors are 2.2 m × 1.5 m and 2.1 m × 1.0 m, respectively. All the windows are triple glazed. The size and orientation of the windows are summarized in Table 2 and Fig. 3.

The building model refers to a single zone envelope. The temperature profile is calculated with the following differential equation [26]:

$$CAP\frac{dT_r}{dt} = \gamma\varepsilon C_{min}(T_i - T_r) + Q_{gain} - UA(T_r - T_{am}) \quad (1)$$

where, CAP is the effective capacitance (kJ/K), T_r is the indoor temperature (°C), C_{min} is the minimum fluid capacitance rate of the heat exchanger (kJ/h K), γ is a coefficient that describes the operation of the entering source stream (1 or 0), ε is the effectiveness of the load heat exchanger, T_i is the temperature of the entering source stream (°C), Q_{gain} is heat gains (kJ/h), UA is the overall loss coefficient (kJ/h K), and T_{am} is ambient temperature outside the structure (°C). The calculation of the internal heat gains has been performed by assuming an average mean internal heat gain from lights, appliances, and occupants of 4 W/m^2 [27]. The differential controller is used to control the operation of the HP, depending on the threshold temperature of the building. The control strategy of on-off is adopted. In order to avoid starting and shutting down the HP frequently, the indoor temperature is assumed to be controlled in the band of 18 ± 2 °C.

Table 1
General information about the detached house model.

Parameter	Unit	Value
Total floor area	m^2	153
Total external wall area	m^2	143
Total windows area	m^2	36
Total heated volume	m^3	375
Ceiling height (ground floor)	m	2.5
Ceiling height (upper floor)	m	2.4
Building Envelope U-value	$W/m^2 K$	0.50
Window SHGC	–	0.68
Window U-value	$W/m^2 K$	1.9
Air tightness	ACH	0.5

Table 2
Windows dimensions.

Reference number from Fig. 3	Size
(19 and 10)	1.45 m × 1.25 m and 1.45 m × 0.62 m
(17–18)	two of 1.45 m × 1.25 m
(14–15)	two of 1.45 m × 1.25 m
(13 and 12)	1.45 m × 1.25 m and 1.45 m × 0.62 m
(11 and 16)	2.6 m × 1.2 m and 2 m × 1.25 m
(1 and 9)	1.45 m × 1.25 and 2 m × 1.25 m
(8 and 7)	2.9 m × 1.25 m and 2 m × 1.25 m
(6)	2 m × 1.25 m
(4–5)	two of 1.45 m × 1.25 m
(3)	0.25 m × 0.96 m
(2)	0.25 m × 0.96 m

2.3. Model of the wind power driven heat pump

The WT-HP is also modelled in TRNSYS® [25]. The main components include: the weather data input block (Type 15), a WT (Type 90), a charge regulator/inverter (Type 48), and a battery bank (Type 47). Three equation blocks are used to describe the HP performance characteristic curve (COP vs ambient temperature), calculate the HP load, the on-off cycle depending on the COP and indoor temperature, and perform the appropriate measurement units conversions. A schematic diagram of the system simulated in TRNSYS® is depicted in Fig. 4.

2.3.1. Model of the heat pump

To estimate the power demand of the HP, an in-house model is developed to simulate its thermodynamic performance at different ambient temperatures in Matlab® [29]. R-410a, as a common working fluid for HPs, is selected. The main objective of the simulation is to find the relationship between COP and outdoor temperature. A fan-coil heat exchanger is selected for the evaporator, and the degree of superheat was 2–4 °C. The isentropic efficiency of the scroll compressor was 80%. It is assumed that the compression ratio has a linear relationship with the ambient temperature [30]. For the condenser, a brazed plate heat exchanger is used and the degree of supercooling is set as 3.5 °C. More details of the developed in-house model can be found in Appendix A. The thermal demand of the building has been thus converted into an electric demand by using the calculated COP equation given in Section 2.4. The rated electrical power of the HP was assumed to be 6 kW_{el}

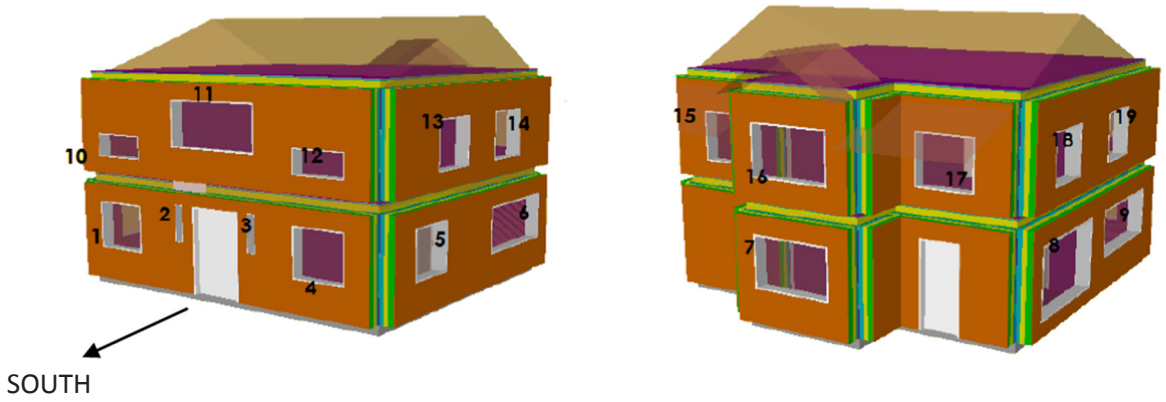

Fig. 3. Windows locations [28].

according to the heat demand and COP of HP at the lowest temperatures. The HP is controlled by an on-off controller.

2.3.2. Model of wind turbine and battery bank

The dynamic simulations of the WT system have been conducted with the following assumptions: if the wind speed is lower than the WT cut-in speed, the power production is null; similarly, if the wind speed exceeds the cut-out speed, the power production is null; and if the wind speed is comprised between the cut-in and cut-out speeds, the power produced is given by the characteristic power curve of the WT. In particular, the WT model simulates three commercially available small WTs: 8 kW_r Viryd [31], 10 kW_r Tozzigreen [32] and 15 kW_r Eolicar [33]. The simulations are performed through the use of the small WTs characteristic power curves, given in Fig. 5, assuming a tower height of 20 m. The weather data refer to Stockholm and were retrieved from Meteonorm database [24].

The battery overcomes the mismatching between power production and consumption. The charge regulator/inverter model manages the energy fluxes between wind power system, battery and HP. The efficiencies of the charge regulator and inverter have been assumed equal to 78% and 96% (default values for Type 48). The used charge regulator and inverter model manage the surplus of power through the simulation of a dumping load. In real applications, typical dumping loads are resistive loads such as air heaters or water heater elements. The heat

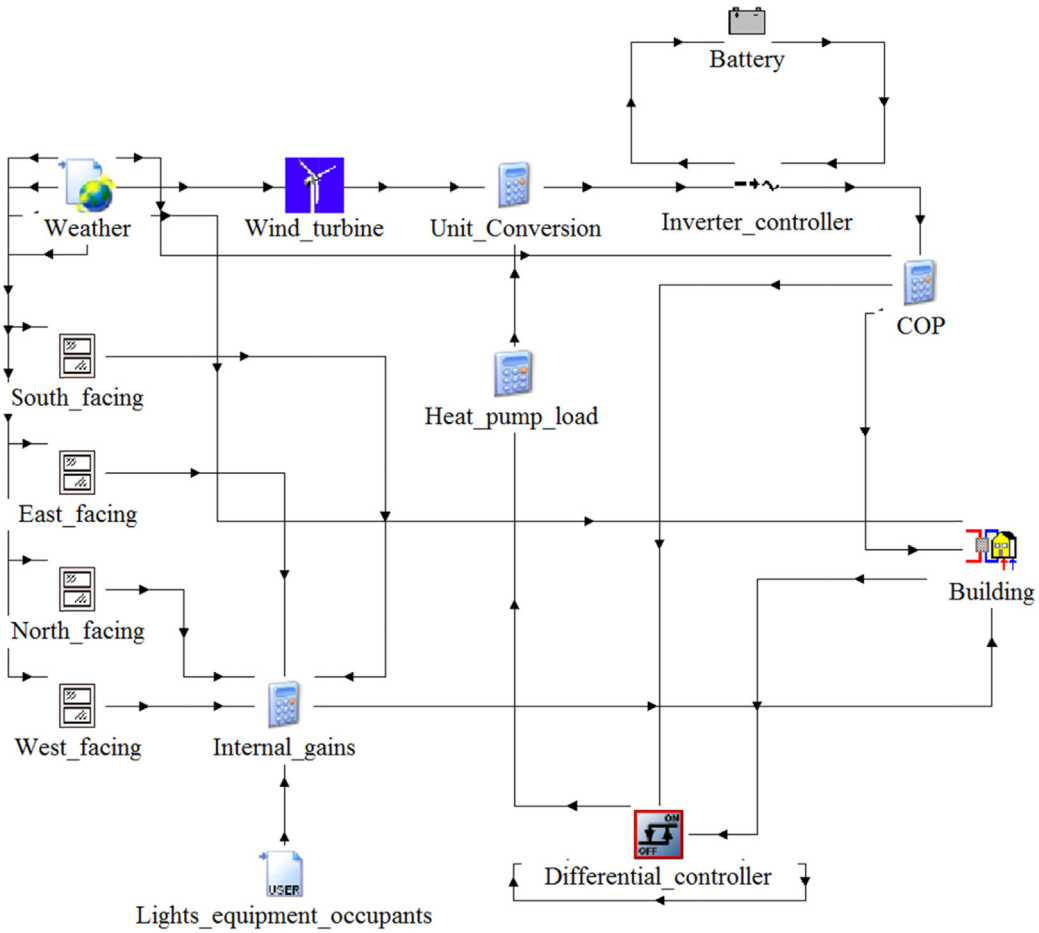

Fig. 4. TRNSYS® schematic model of the detached house and wind power driven heat pump system for space heating.

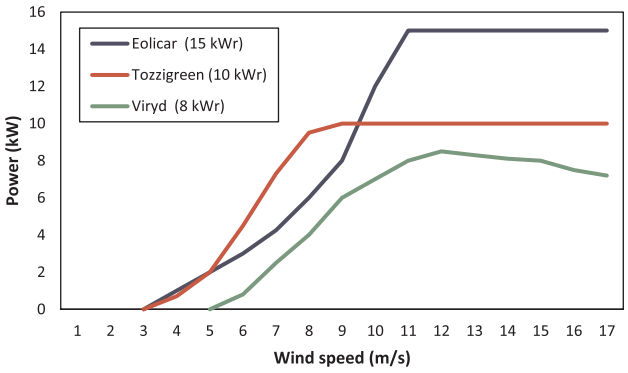

Fig. 5. Characteristic power curves of the simulated small wind turbines [31–33].

generated by resistive loads can be dissipated or stored in hot water tanks for domestic hot water. The battery model implemented in this study performs an energy balance between energy input, output and stored. The round trip efficiency has been set to 90% (default value for Type 47). Five battery capacities have been taken into consideration in this study: 10, 20, 30, 40, and 50 kWh. The system investigated in this study is off-grid. In real applications, the overall heating demand is met by using thermal back-up systems such as wood or gas boilers, or micro-CHP systems, such as wood powered Stirling engines.

The sensitivity analyses conducted in this study have considered the following sensitive parameters: small WT rated capacity, battery capacity, setpoint of indoor temperature and related intervals, and simulation time step.

2.4. Models validation

2.4.1. Heat pump model

For the validation of the HP model, COPs at different ambient temperatures were compared with the product specification given by some HPs companies [34–37]. The good agreement, with data from references comprised within ± 10% of the obtained simulation results (Fig. 6), clearly shows that the developed model can be used to assess the electricity consumption of the HP.

Based on this model, the COP was correlated to the ambient temperature by using the following equation:

$$COP = 2.79 + 0.036 \times T_{am} + 6.036 \times 10^{-4} \times T_{am}^2 \quad (2)$$

where, T_{am} (°C) is the ambient temperature. When the heat demand is obtained from the house model, the corresponding power demand can

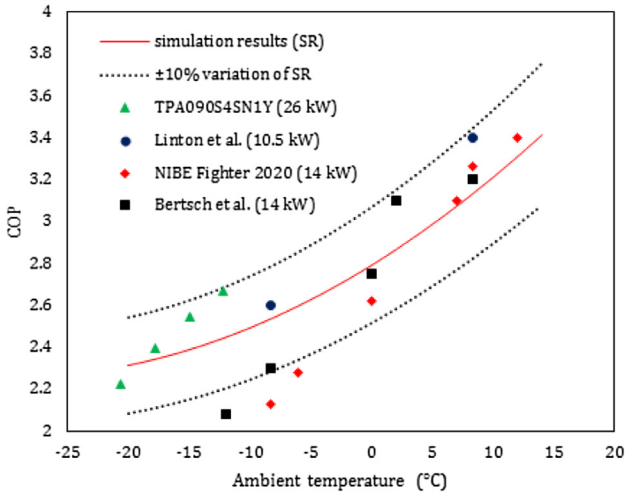

Fig. 6. Validation of the heat pump model.

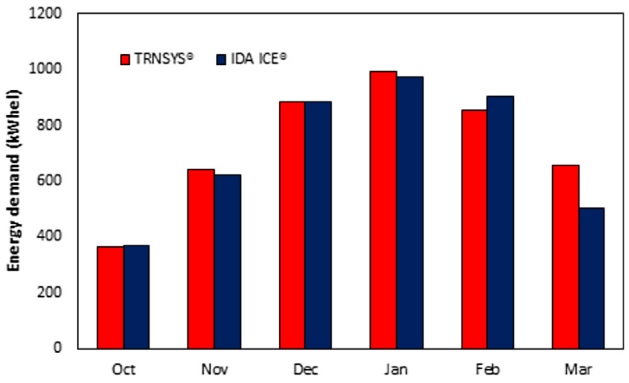

Fig. 7. Comparison between house heating demand performed with TRNSYS® Type 12 and IDA ICE®.

be estimated by using this correlation. It is important to highlight that the minimum temperature at which a HP can operate efficiently can vary according to the system design and selected working fluids. For the worst situation, the HP will operate like an electrical heater. In this paper, it is assumed that when the ambient temperature is below −20 °C, the COP of HP is 1.

2.4.2. Building model

Persson et al. compared Type 12 with Type 56 for a reference building connected to the IEA Task 32 [38]. The results of the comparison showed that Type12 was marked out by a percentage error lower than 7% for 90% of the annual heating load. A further validation of the model has been performed by comparing the results with those from a model developed in IDA ICE® [39]. As it can be seen in Fig. 7, a good agreement was obtained.

2.4.3. Wind turbine model

The validation of the WT model was performed through wind power measurements carried out at a small WT installed in Köping, Sweden. The small WT model is Kestrel e300i. It is mounted on an 18 m tower and the power capacity is 1 kW_r. At a height of 10 m above ground, a weather station from Lufft [40], model WS600 Ultrasonic Weather Station, is installed on a transversal beam. Fig. 8 shows the WT used for the measurements and validation of the dynamic simulations together with the system layout. The dynamic simulations have been compared with the measurements performed during January 2013, as shown in Fig. 9. Good agreements can also be observed.

2.4.4. Battery model

Zhang et al. compared the battery energy balance model, similar to the model implemented in Type 47, to the improved Shepherd model for the calculation of the state of charge (SOC) of the battery [41]. Similar results were obtained.

2.5. Key performance indicators

In order to evaluate the performance of the WT-HP, two key performance indicators are proposed in this work:

- the loss of load probability (LOLP), a measure of the probability that the energy demand will exceed the energy supply during a given period. It is defined as:

$$LOLP = \frac{\sum t_{lol}}{t_{total}} \quad (3)$$

where, t_{lol} is the number of time steps when the energy output from WP is lower than the energy demand of HP and t_{total} is the total number of time steps of the studied period;

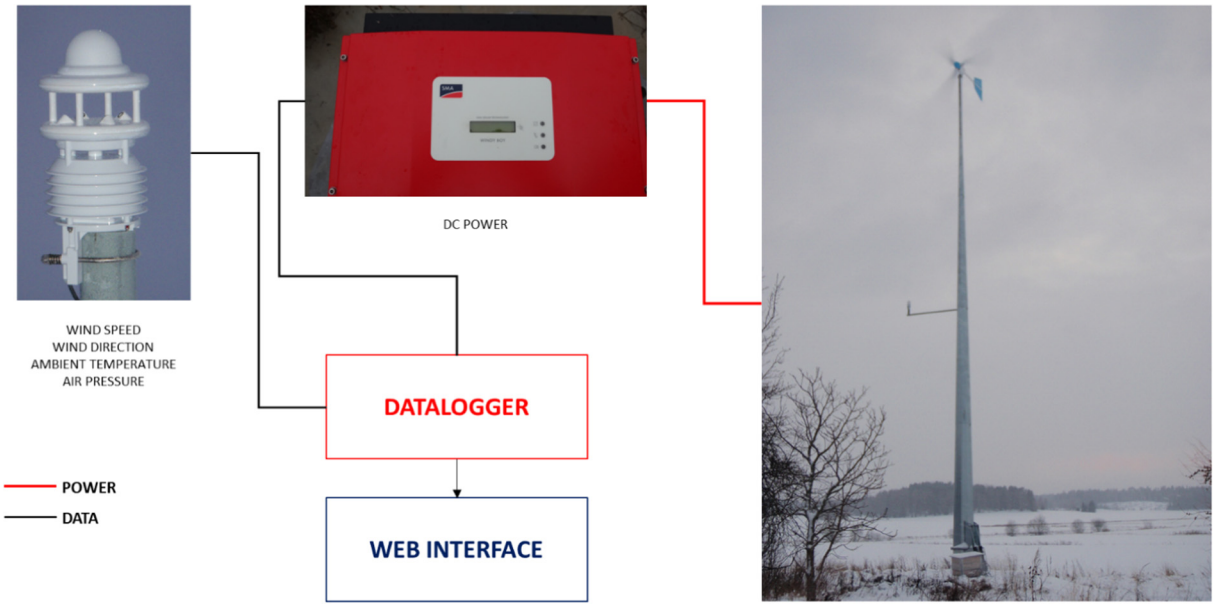

Fig. 8. Wind power and wind speed measurements test bench.

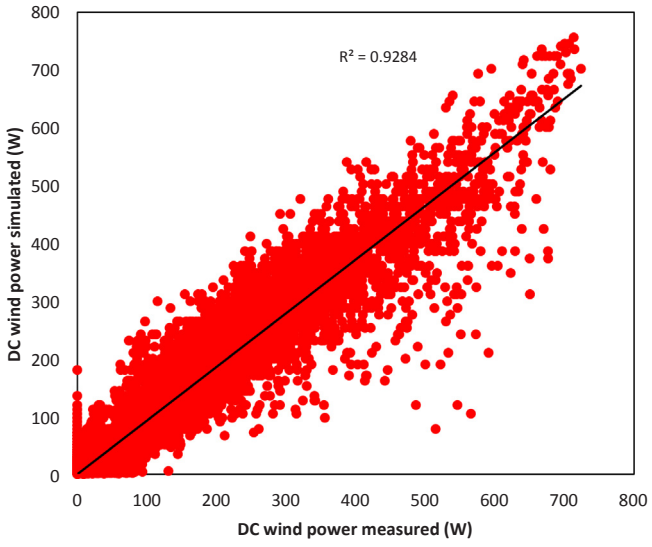

Fig. 9. Measured and simulated DC power.

- the loss of thermal comfort probability (LOTCP), a measure of the probability that the indoor temperature is lower than the setpoint temperature during a given period. It is defined as:

$$LOTCP = \frac{\sum t_{lotc}}{t_{total}} \tag{4}$$

where, t_{lotc} is the number of time steps when the indoor temperature is lower than the setpoint temperature.

The thermal comfort is affected by several factors, both human related and environment related, such as metabolic rate, clothing level, indoor ambient temperature, radiant temperature, air speed and humidity. This study mainly focused on the indoor temperature, which is the most important parameter for the thermal comfort, especially during the winter heating season. This assumption is due to the energy consumption is mainly determined by the difference between average outdoor and indoor temperatures.

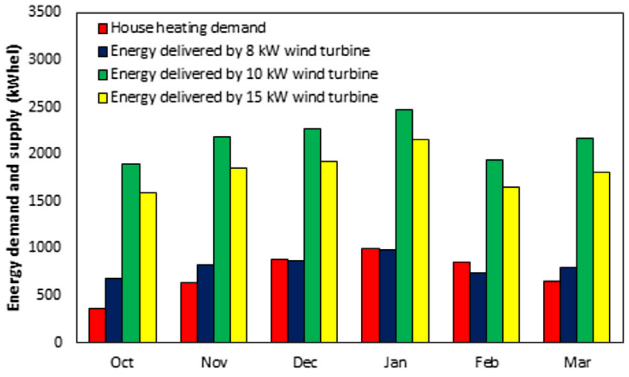

Fig. 10. Heating energy demand of the detached house and energy supply of the wind turbines.

3. Results and discussion

3.1. Overall performance

The monthly average energy demand of the house is illustrated in Fig. 10. The energy demand refers to space heating; while the energy consumption for DHW, lighting, cooking and other electronic appliances, such as washing machines, TV and fridges, is not considered in this work. The need of space heating increases along the drop of the ambient temperature. Since January has the lowest monthly average ambient temperature, it has the highest energy demand. The monthly energy outputs of the chosen three WTs with different capacities are also shown in Fig. 10. The 8 kW_r WT could not fully satisfy the energy demand of the HP during the heating season. Despite the higher rated power, the power output of the 15 kW_r WT is lower than that of the 10 kW_r WT. More discussions related to the WT power outputs are given in Section 3.2. Considering the intermittent characteristic of the wind power, it is of great importance to perform dynamic simulations when studying the feasibility of the WT-HP. Fig. 11 compares the energy demand and energy supply from the 10 kW_r WT at 1-min time step. Obviously, during some time steps the energy output of the WT exceeds the demand; while during some other time steps there is not enough energy output. The calculated LOLP is 59.9%, which is quite high. In order to improve the system performance, the extra energy output can

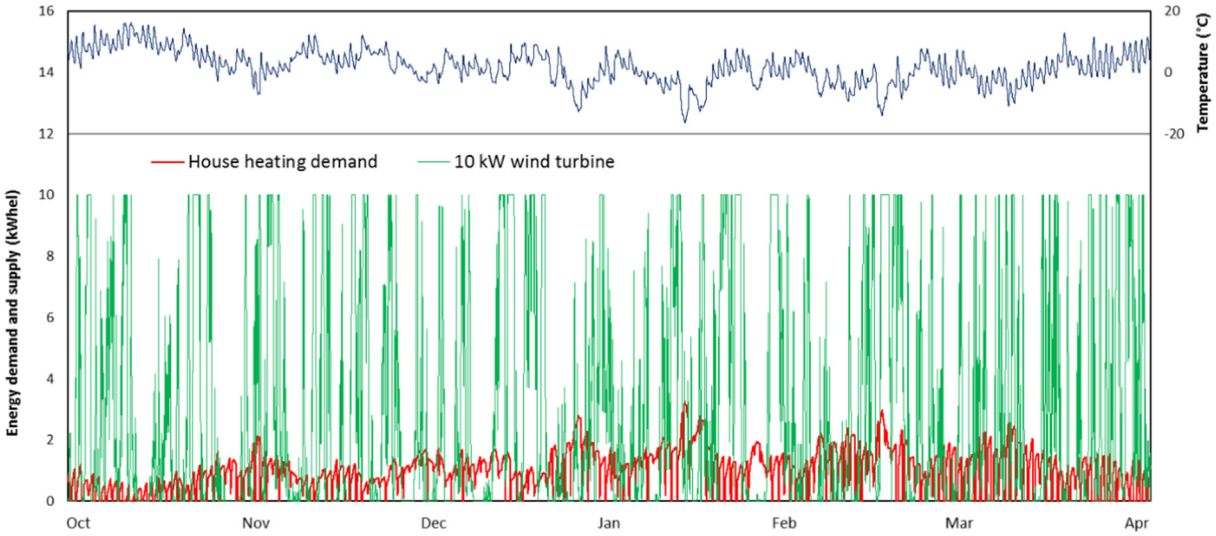

Fig. 11. Energy demand for space heating, energy supplied by the 10 kW_r wind turbine, and ambient temperature.

be stored and used when there is insufficient energy output from the WT. A battery bank of 20 kWh is assumed. After the battery bank is integrated, the LOLP can be reduced down to 35.8%.

The thermal comfort, which is reflected by the indoor temperature, is important for space heating. A good thermal comfort intends to keep the indoor temperature stable and in the desired temperature band. Although the indoor temperature is clearly affected by the operation of the HP, which is further affected by the energy output of the WT, LOTCP may not be consistent to the LOLP due to the heat capacity of the building. Therefore, it is also essential to calculate the LOTCP. Fig. 12 shows the variation of indoor temperature for the systems consisting of a 10 kW_r WT without and with a 20 kWh battery. For the system without battery, the LOTCP is about 48.4%. It implies that the number of time steps during the period from October to March, in which the indoor temperature is lower than 16 °C, corresponds to about 3000 h. The introduction of the battery can reduce the LOTCP. For example, a battery of 20 kWh can reduce the LOTCP down to 32.0%. Meanwhile, the battery can also increase the average indoor temperature, from 14.5 °C to 15.6 °C.

3.2. The influence of wind turbine capacity

To improve the system performance, which means reducing the LOLP and LOTCP, one way is to increase the installed capacity of the WT, which can potentially convert more energy. The dynamic simulations of the wind energy output from 10 kW_r and 15 kW_r WTs are depicted in Fig. 13. It is interesting to see that the 15 kW_r WT does not always produce more electricity than the 10 kW_r WT, as it can be seen from Fig. 5, due to the different WT power curves. From the wind frequency distribution depicted in Fig. 14, it can be seen that most of the wind speeds at the chosen location are comprised between 0 and 8 m/s. In this wind speed range, the power curve of the 10 kW_r WT always shows better performances compared to the 15 kW_r WT. As a result, the 15 kW_r WT produces less electricity than the 10 kW_r WT during October to March at the specified hub height. The LOLP and LOTCP are also estimated for the system consisting of a 15 kW_r WT and a 20 kWh battery, which are 43.2% and 36.0%. It is clear that compared to the system equipped with a 10 kW_r WT and the same battery capacity, both the LOLP and LOTCP are higher (35.8% and 32.0%, respectively). While, this study has focused on an off-grid system, nevertheless, the introduction of WT-HP in an on-grid configuration, for

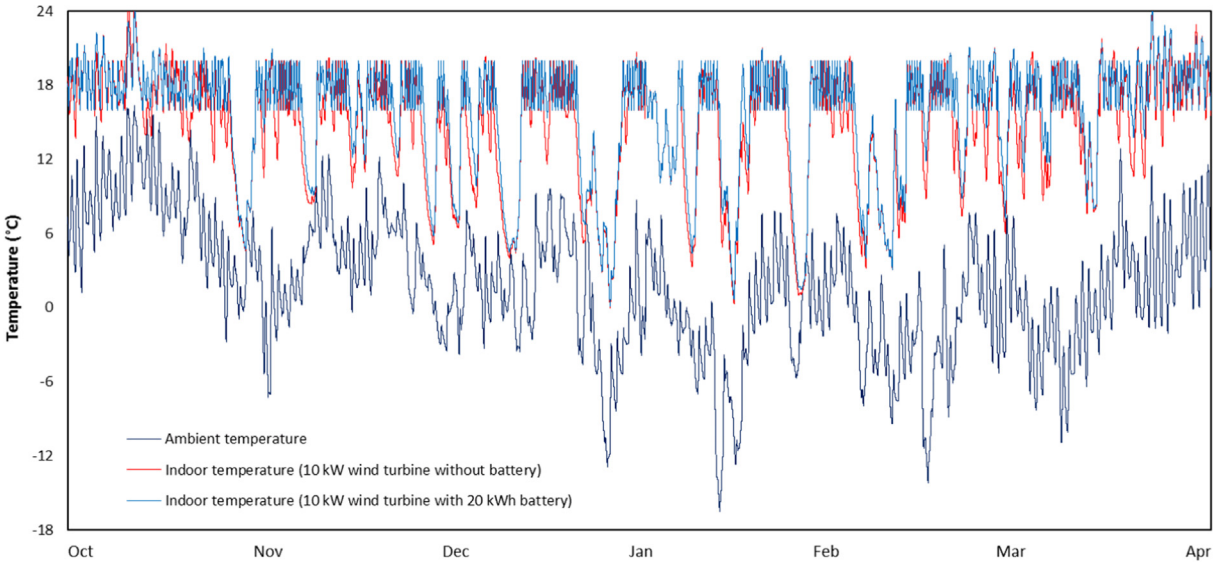

Fig. 12. Fluctuation of the indoor temperature.

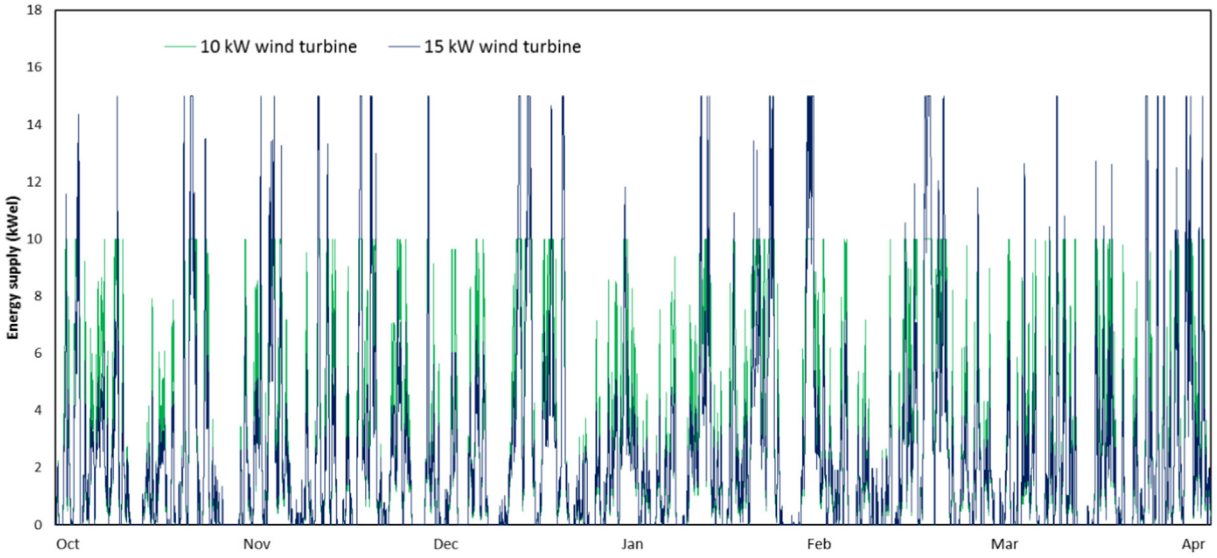

Fig. 13. Energy supply from two wind turbines with capacities of 10 kW_r and 15 kW_r.

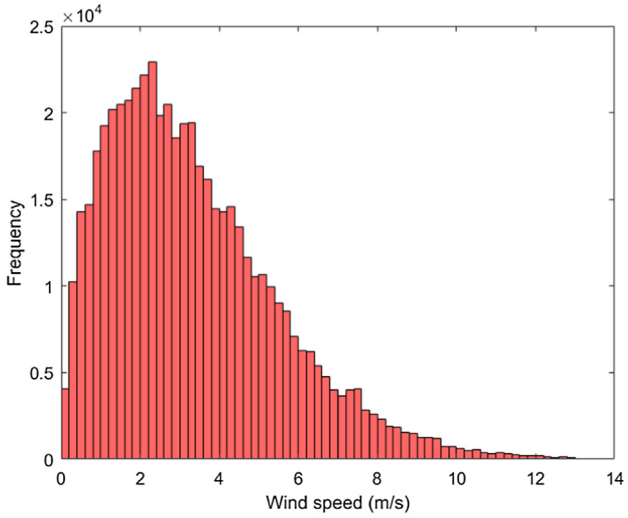

Fig. 14. Wind speed distribution (1 min time step).

example in connection to a district heating, can reduce the peak load of district heating. This can be easily understood from Fig. 1, since high wind speeds and thus high wind power productions coincide with low ambient temperatures, which imply a high heat demand. The WT energy surplus can be stored in electrical energy storage systems. It can also be converted to heat, which can be stored in thermal energy storage systems or injected into the district heating network.

3.3. The influence of the desired indoor temperature

The heat demand is tightly dependent on the desired indoor temperature. Therefore, the system performance can also be influenced by the indoor temperature. Assuming a 10 kW_r WT connected to the HP, when the desired indoor setpoint temperature is increased from 18 ± 2 °C to 20 ± 2 °C, the LOLP increases from 59.9% to 62.6% whereas the LOTCP increases from 48.4% to 56.7%. By increasing the indoor temperature, the LOLP increases since the power required to keep a higher indoor temperature increases. As a result, there is a longer time, in which the indoor temperature is lower than the setpoint temperature. Accordingly, the LOTCP increases because the WT can meet the heat demand, and thus the indoor temperature, for a shorter time compared to the previous case. Fig. 15 shows the indoor temperature profiles for two different desired indoor temperatures. The variation of indoor temperatures is similar, but it has a larger amplitude for the setpoint temperature case of 20 ± 2 °C.

3.4. The influence of the battery capacity

Another way to improve the system performance is to increase the battery capacity. Increasing the battery capacity can effectively reduce the dumped power; therefore, both LOLP and LOTCP can be lowered. To understand the influence of battery capacity, other battery capacities are tested: 10, 30, 40, and 50 kWh. A summary of the LOLP and LOTCP as a function of the battery capacity is given in Fig. 16. Naturally, LOLP can be effectively reduced by increasing the capacity of the battery, as much more dumped electricity can be stored and utilized. Consequently, lower LOTCP could also be achieved.

3.5. The influence of time interval on the dynamic simulation

To understand the influence of the time step on the accuracy of the simulations, simulations were performed by using 1 h as time step. The fluctuation of indoor temperatures at 1 h time step is shown in Fig. 17 for different setpoint temperatures (18 ± 2 °C and 20 ± 2 °C). Even though ± 2 °C was assumed for the operation control of the heating system, it is clear that the highest indoor temperatures went over 18 ± 2 °C and 20 ± 2 °C. Contrarily, it is shown in Fig. 15 that the highest temperature is limited to the defined setpoint temperatures. The reason mainly comes from the time interval used in the dynamic simulation. If the HP is working for 1 h, it may produce more heat than required, resulting in an indoor temperature higher than the setpoint.

Different temperatures at different time steps imply that the LOTCP is also influenced by the time interval as well. Besides the energy output from the WTs, the operation of the HP is also affected by the energy stored in the batteries. Principally, a larger capacity can store more energy. Nevertheless, the real stored energy is also dependent on the simulation interval. The wind speed normally varies continuously; however, when using 1 h as time step, average wind speed is used, which becomes discrete. Therefore, in the period the wind speed varies more frequently, it can happen that the system consisting of a 30 kWh battery is charged less often and consequently, has a higher LOTCP. Those issues can be avoided by using a higher time step resolution. The simulations in Section 3.4 were performed by using 1 h interval. The results, summarized in Table 3, show that both the LOLP and LOTCP become smaller as a larger capacity of battery is used. In addition, it is

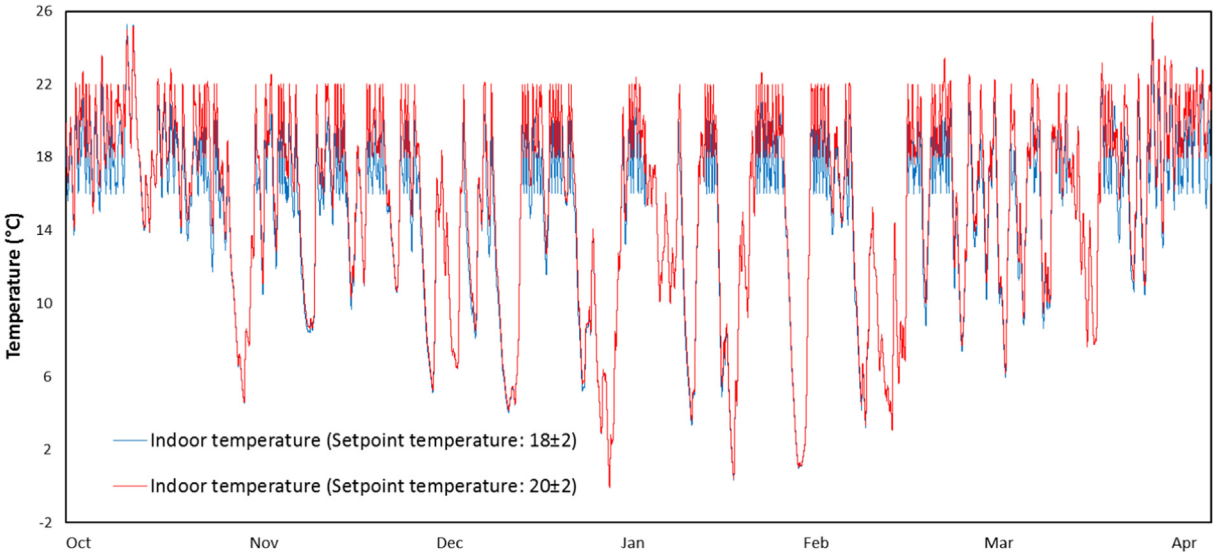

Fig. 15. Fluctuation of the indoor temperature at different setpoint temperatures.

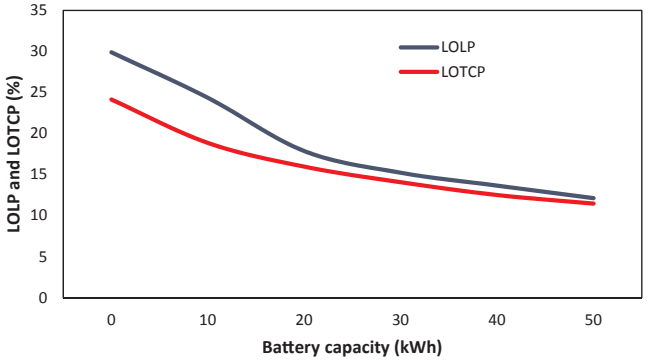

Fig. 16. Effects of the battery capacity on the LOLP and LOTCP.

clear that both the LOLP and LOTCP are generally lower at high battery capacity and higher time resolution since the operation can be simulated in a more precise way by capturing the dynamic behaviour of the heat supply and indoor temperature.

Table 3
LOLP and LOTCP at different time intervals used in the dynamic simulations with 10 kW_r WT.

Battery capacity (kWh)	LOLP		LOTCP	
	1 min	1 h	1 min	1 h
0 kWh	59.9%	49.4%	48.4%	46.4%
10 kWh	48.8%	46.6%	37.8%	45.0%
20 kWh	35.8%	36.4%	32.0%	40.7%
30 kWh	30.5%	31.1%	28.2%	38.5%

4. Conclusions

This paper studied the dynamic performance of a heat pump system directly driven by wind turbine. The heat demand of a detached single family house, the energy from the wind turbines and the fluctuation of indoor temperature were simulated. Based on the results, the following conclusions were drawn:

- Due to the intermittent characteristic of wind energy, the wind

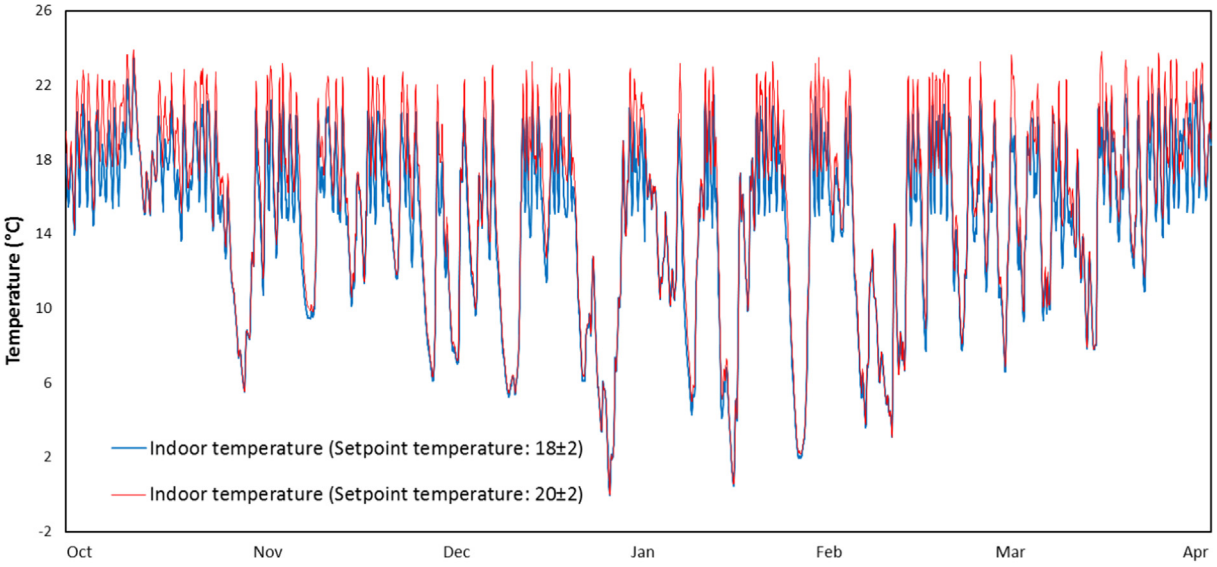

Fig. 17. Fluctuation of the indoor temperatures when using 1 h as time step.

turbine cannot fully satisfy the electricity demand of the heat pump;
- Increasing the capacity of the wind turbine does not necessarily lead to a higher electrical energy output due to the matching between wind speeds and the wind turbine power curve. In the studied location and at the selected turbine height, the selected 10 kW_r wind turbine converts more energy than the 15 kW_r wind turbine. By increasing the wind turbine capacity, it resulted in a higher loss of load probability and a higher loss of thermal comfort probability;
- Since energy surplus also exists, the extra electricity generation can be stored in energy storage systems. Thus, including a battery system can effectively lower both the loss of load probability and loss of thermal comfort probability. For example, the 10 kW_r wind turbine with a battery bank of 20 kWh could reduce the loss of load probability from 59.9% to 35.8%, compared to the system without battery. Similarly, the loss of thermal comfort probability for system without battery was about 48.4% while the introduction of the 20 kWh battery could reduce the loss of thermal comfort probability down to 32.0%;
- By choosing a setpoint temperature of 20 ± 2 °C, the loss of load probability increased from 59.9% to 62.5% whereas the loss of thermal comfort probability increased from 48.4% to 56.7%;
- The time interval used in the dynamic simulation has significant influence on the results, especially on the loss of thermal comfort probability. In order to have more accurate results, it is thus of great importance to choose a high resolution time step to capture the dynamics of the thermal behaviour of the building. By decreasing the simulations temporal resolution from 1 min to 1 h, the loss of load probability and the loss of thermal comfort probability tended to increase. For the case of 10 kW_r wind turbine with 10 kWh battery, the loss of thermal comfort probability increased from 37.8% to 45%.

Acknowledgements

This work was supported by National High-Technology Research and Development Program ("863" Program) of China (2015AA050403). The authors acknowledge the financial support from J. Gust. Richert Foundation, and the Swedish Knowledge Foundation (KKS) research profile Future Energy at Mälardalen University. The authors also acknowledge the help received by Sven Ruin for performing the wind power and wind speed measurements. The author Yuting Tan acknowledges the financial support from China Scholarship Council (CSC).

Appendix A. Heat pump model

A.1. Working principle

HP mainly consists of four components: an evaporator, a compressor, a condenser and an expansion valve. Mechanical HPs exploit the physical properties of a volatile evaporating and condensing fluid known as a refrigerant.

A.2. Working fluid R-410A

R-410A is a highly efficient nearly azeotropic mixture (gases evaporate at nearly the same temperatures) of two gases (50vol% of R-32 and 50vol % of R-125). R-410A is a long-term green alternative refrigerant with zero ozone-depleting-potential (ODP) to replace R-22, ideally suited for replacing R-22 in scroll compressor packages. R-410A can find increasingly wide application in residential air conditioners in Europe. Table 4 lists some properties of R-410A [42].

A.3. Simulation procedure

The main objective of the simulation of the HP is to find the relationship between performances of the HP with the ambient temperature, specifically, with the variation of ambient temperature. The flowchart of simulation is given in Fig. A.1.

In details, the simulation procedure has considered the following aspects:

(1) For the evaporator, air-R-410A fin-coil heat exchanger is chosen, the outer area is 26.3 m^2, the inner area is 2.63 m^2, and the heat transfer coefficient of the air side is calculated as 25–35 $W/m^2/K$ [43–46]. The degree of superheat (DSH) is set as 2–4 °C.
(2) In the HP system, Copeland scroll compressor ZH21K4E-TFD is chosen, which has isentropic efficiency of 80% [47]. According to the experiments, the compression ratio of the compressor has a linear relationship with ambient temperature, and then the discharge pressure can be calculated as described in [48]. There are three key parameters that are of interest in the compressor model: mass flow rate (m_c), outlet enthalpy ($H_{c,out}$), and input power (W_c), which are given by following equations respectively:

$$m_c = \omega_c V_c \rho_c \eta_{vol} \tag{A.1}$$

$$H_{c,out} = \frac{1}{\eta_{ise}}(H_{c,out,ise} - H_{c,in}(1-\eta_{ise})) \tag{A.2}$$

Table 4
Property of R-410A [42].

Property	Value
Formula	50% R32/50% R125
Molecular Weight (Da)	72.6
Critical temperature (°C)	72.8
Critical pressure, MPa	4.86
Gas heat capacity (kJ/(kg °C))	0.84
Liquid heat capacity @ 1 atm, 30 °C, (kJ/(kg °C))	1.8
ODP	0
GWP	1725

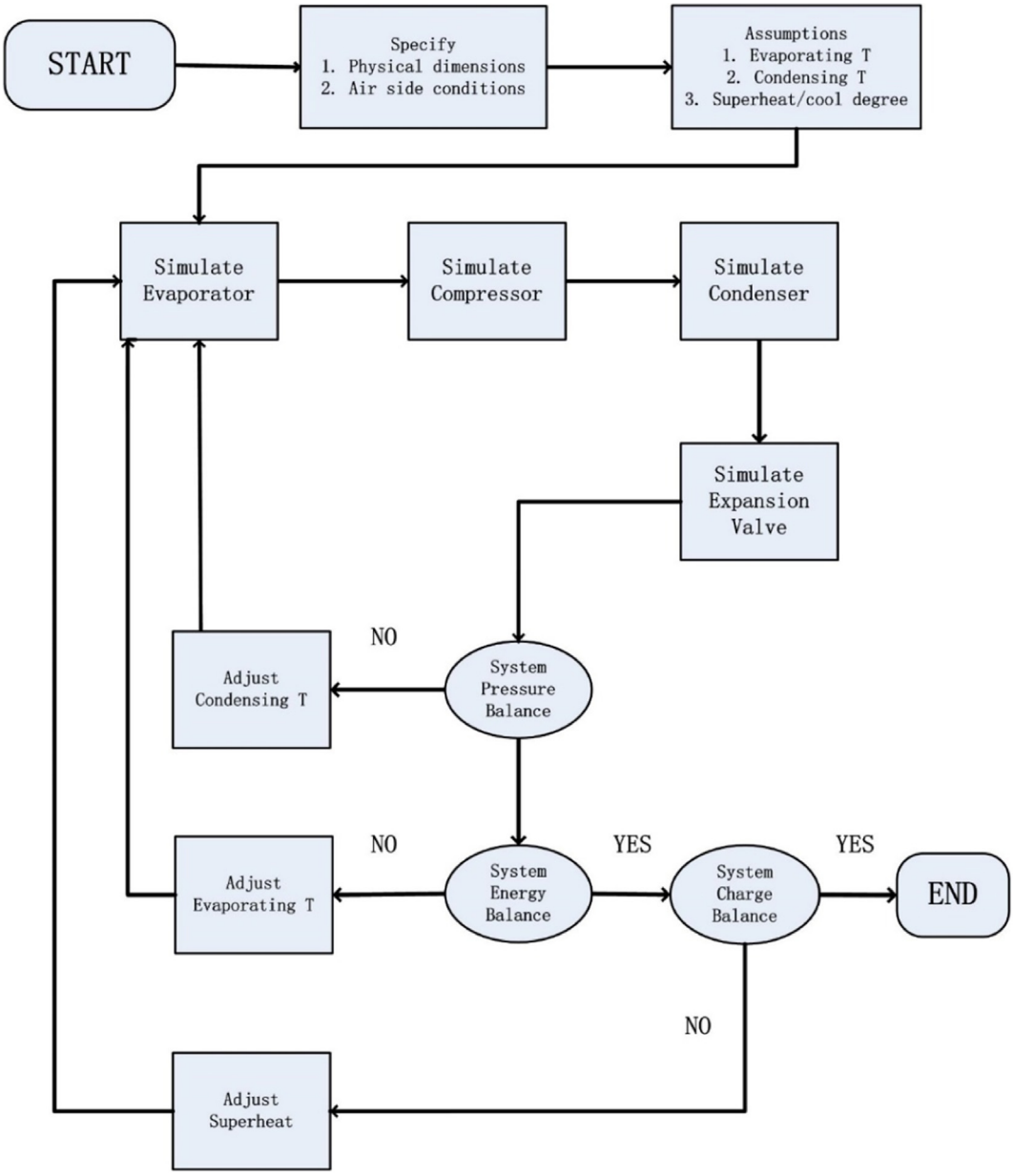

Fig. A.1. Simulation algorithm flowchart.

$$W_c = \frac{m_c(H_{c,out} - H_{c,in})}{\eta_{mec}\eta_{ele}} \tag{A.3}$$

where, ω_c and V_c are the rotation speed and displacement of the compressor; ρ_c is the inlet density of the gas; η_{vol} and η_c are the volumetric efficiency and isentropic efficiency of the compressor; and η_{mec} and η_{ele} are the mechanical and electric efficiencies of the compressor.

(3) For the condenser, Alfa CB62/CBH62 brazed plate heat exchanger (Brine/water style) is chosen. In the condensation process, the pressure can be treated as constant regardless of the pressure drop. In this simulation, the degree of supercooling (DSC) is set constant (3.5 °C). The condenser is divided into three zones, namely superheating, two-phase, and subcooled zones. Lumped parameters are considered in each zone. The heat transfer rate (q_{c1}), the outlet water temperature (T_{w1o}) and the area of superheating zone (A_{c1}) are calculated from the following equations:

$$q_{c1} = m_r(H_{ci} - H_{cg}) \tag{A.4}$$

$$T_{w1o} = T_{w1i} + \frac{q_{c1}}{Cp_w} \tag{A.5}$$

$$A_{c1} = \frac{q_{c1}}{U_{c1}LMTD_{c1}} \tag{A.6}$$

$$LMTD_{c1} = \frac{(T_{ci} - T_{wi}) - (T_{co1} - T_{wo1})}{\ln(\frac{T_{ci} - T_{wi}}{T_{co1} - T_{wo1}})} \quad (A.7)$$

where, Cp_w is the heat capacity of water; and U_{c1} *and* $LMTD_{c1}$ are the heat coefficient and logarithmic temperature difference of the superheating zone of the condenser.

The heat transfer rate (q_{c2}), the outlet water temperature and the area of the two-phase region are calculated in the same way as that of superheating phase. The area of the subcooled zone is deduced from the previous areas, then the number of transfer units (*NTU*) and effectiveness (ε) of this zone, and the maximum and actual heat transfer rates (εq_{c3max} *and* q_{c3}) are calculated with the following equations:

$$NTU = \frac{U_{c3}A_{c3}}{C_{min}} \quad (A.8)$$

$$\varepsilon = \frac{1 - e^{-NTU(1+C)}}{1 + C} \quad (A.9)$$

$$q_{c3,max} = C_{min}(T_{c3i} - T_{w3i}) \quad (A.10)$$

$$q_{c3} = \varepsilon q_{c3,max} \quad (A.11)$$

(4) As for the expansion process, there are two key parameters calculated from the valve model: the mass flow rate (m_c) and the outlet enthalpy ($h_{v,out}$), which are given by the following equations:

$$m_c = C_d\sqrt{\rho(P_{in} - P_{out})} \quad (A.12)$$

$$h_{v,in} = h_{v,out} \quad (A.13)$$

where, P_{in} and P_{out} are inlet and outlet pressure of the expansion valve.

(5) following the aforementioned procedures, the performance can be assessed. The theoretical coefficient of performance (COP) is calculated as follows: COP = Q_c/W_c, where, Q_c is the heat duty of the condenser and W_c is the energy consumption in the compressor.

References

[1] IEA, World Energy Outlook; 2012.
[2] DOE, Buildings energy data book. Available at: https://openei.org/doe-opendata/dataset/buildings-energy-data-book. [accessed: 13th September 2017].
[3] Värmemarknad, The heating market in Sweden, 2014.
[4] Molin A, Rohdin P, Moshfegh B. Investigation of energy performance of newly built low-energy building in Sweden. Energy Build 2011;43:2822–31.
[5] Svensk Vindenergi – Swedish Energy Association (SWEA), Statistics and forecast (Q4 2017); 2018 https://svenskvindenergi.org/wp-content/uploads/2018/02/Statistics-and-forecast-Svensk-Vindenergi-20180216.pdf [accessed: 20th, May 2018].
[6] Waite M, Modi V. Potential for increased wind-generated electricity utilization using heat pumps in urban areas. Appl Energy 2014;135:634–42.
[7] Hedegaard K, Mathiesen BV, Lund H, Heiselberg P. Wind power integration using individual heat pumps – analysis of different heat storage options. Energy 2012;47(1):284–93.
[8] Meibom P, Kiviluoma J, Barth R, Brand H, Weber C, Larsen H. Value of electric heat boilers and heat pumps for wind power integration. Wind Energy 2007;10:321–37.
[9] Warmer C, Hommelberg M, Kamphuis I, Derzsi Z, Kok J. Wind turbine and heat pumps – balancing wind power fluctuations using flexible demand. In: Sixth international workshop on large-scale integration of wind power on transmission networks from offshore wind farm, 26–28 October 2006, Delft, the Netherlands.
[10] Fischer D, Madani H. On heat pumps in smart grids: a review. Renew Sustain Energy Rev 2017;70:342–57.
[11] Poulet P, Outbib R. Energy production for dwellings by using hybrid systems based on heat pump variable input power. Appl Energy 2015;147:413–29.
[12] Papaefthymiou G, Hasche B, Nabe C. Potential of heat pumps for demand side management and wind power integration in the German electricity market. IEEE Trans Sustain Energy 2012;3:636–41.
[13] Jwo C, Chien Z, Chen Y, Chien C. Development of a wind directly forced heat pump and its efficiency Analysis. Int J Photoenergy 2013. Article ID 862547.
[14] Braymer J, Pinotti M, Dybbs A. A wind powered heat pump. In: Yuan SW, editor. Energy, resources and environment. Pergamon; 1982. p. 528–35.
[15] Zhang Y, Gu J. Analysis on operation characteristics of wind source heat pump system. Adv Mater Res 2012;608–609:818–21.
[16] Li Q, Chen Q, Zhang X. Performance analysis of a rooftop wind solar hybrid heat pump system for buildings. Energy Build 2013;65:75–83.
[17] Li H, An Q, Yu B, Zhao J, Cheng L, Wang Y. Strategy analysis of demand side management on distributed heating driven by wind power. Energy Proc 2017;105:2207–13.
[18] Østergaard P. Wind power integration in Aalborg Municipality using compression heat pumps and geothermal absorption heat pumps. Energy 2013;49:502–8.
[19] Sichilalu S, Tazvinga H, Xia X. Optimal control of a fuel cell/wind/PV/grid hybrid system with thermal heat pump load. Sol Energy 2016;135:59–69.
[20] Sichilalu S, Tazvinga H, Xia X. Optimal control of a wind–PV-hybrid powered heat pump water heater. Appl Energy 2017;185:1173–84.
[21] Chemekov VV, Kharchenko VV. The heat supply system for a self-contained dwelling house on the basis of a heat pump and wind power installation. Therm Eng 2013;60:212.
[22] Thygesen R, Karlsson B. Simulation and analysis of a solar assisted heat pump system with two different storage types for high levels of PV electricity self-consumption. Sol Energy 2013;103:19–27.
[23] Thygesen R, Karlsson B. Economic and energy analysis of three solar assisted heat pump systems in near zero energy buildings. Energy Build 2013;66:77–87.
[24] Meteonorm. www.meteonorm.com [accessed: 21st April 2017].
[25] TRNSYS. www.trnsys.com [accessed: 21st April 2017].
[26] ASHRAE, 2001. Handbook of Fundamentals. American Society of Heating, Refrigerating and Air-Conditioning Engineers, Atlanta.
[27] Janson U. Passive houses in Sweden-Experiences from design and construction phase. Licentiate thesis; 2008. ISSN 1651-8136.
[28] Berretta S. Feasibility study of using wind power driven heat pump to supply heat for a single house. Master Thesis at Mälardalen University (2013). Available at: http://www.diva-portal.org/smash/get/diva2:679376/FULLTEXT01.pdf [accessed: 1st September 2017].
[29] Matlab. www.mathworks.com [accessed: 1st September 2017].
[30] Huang H, Qin Z, Li Q, Yuan D. Heating performance analysis of air-source heat pump chiller with refrigerant R410A at varied environment temperature. Cryogenics 2008;1:45–9.
[31] Roadman J, Murphy M, van Dam J. Power performance test report for the Viryd CS8 Wind Turbine; 2012. www.nrel.gov/docs/fy13osti/56500.pdf [accessed: 21st April 2017].
[32] TOZZIgreen. www.tozzigreen.com [accessed: 21st April 2017].
[33] Eolicar. www.eolicar.it. Accessed: 21st April 2017.
[34] Bertsch SS, Groll EA, Bouffard DB, Hutzel WJ. Air source heat pump for northern climates part II: measurement and verification. International Refrigeration and Air Conditioning Conference, July 17–20. USA: Purdue University; 2006.
[35] Environmental Installations Ltd, Air/water heat pump NIBE FIGHTER 2020 Air/water heat pump; 2010.
[36] Air Conditioning & Heating Equipment, Split system commercial heat pumps R-410A/Allied Commercial Heating & Air Conditioning Products, 2005.
[37] Linton JW. Performance of R-22, R-407C AND R-410A at constant cooling capacity in a 10.0 seer 10.5 kW residential central heat pump. In: International refrigeration and air conditioning conference, USA- July 25–28; 2000.
[38] Persson H, Perers B, Carlsson B. Type12 and Type56: a load structure comparison in TRNSYS. In: World Renewable Energy Congress 8–13th May 2011, Linköping, Sweden; 2011.
[39] IDA ICE. www.equa.se/en/ida-ice [accessed: 1st September 2017].
[40] Lufft. www.lufft.com [accessed: 1st September 2017].
[41] Zhang Y, Campana PE, Lundblad A, Wang L, Yan J. The influence of photovoltaic models and battery models in system simulation and optimization. Energy Proc 2017;105:1184–91.
[42] REFPROP-NIST Reference Fluid Properties version 9.1; 2012.

[43] Cavallini A. Experimental investigation on condensation heat transfer and pressure drop of new HFC refrigerants (R134a, R125, R32, R410A, R236ea) in a horizontal smooth tube. Int J Refrig 2001;24:73–87.
[44] Park Chang Yong. Experimental and numerical study on micro channel and round-tube condensers in a R410A residential air-conditioning system. Int J Refrig 2008;31:822–31.
[45] Goto M. Condensation and evaporation heat transfer of R410A inside internally grooved horizontal tubes. Int J Refrig 2001;24:628–38.
[46] Wellsandt S. Evaporation of R407C and R410A in a horizontal herringbone micro fin tube: heat transfer and pressure drop. Int J Refrig 2005;28:901–11.
[47] Emerson Climate Technology, Scroll compressors for air-conditioning-Application Guidelines, 2003.
[48] Huang Hu. Heating performance analysis of air-source heat pump chiller with refrigerant R410A at varied environment temperature. Cryogenic 2008;1:45–9.